

# Greenhouse Gas Emissions during Oil Shale Crushing and Its Main Controlling Factors: A Contrast Study of Oil Shale in Yaojie and Fushun Areas, China

Lijuan Wang,\* Yingxin Lu, Guojun Chen, Lianhua Xue, Zhongning Zhang, Shuan Wang, and Jian Gao



Cite This: *ACS Omega* 2024, 9, 17491–17505



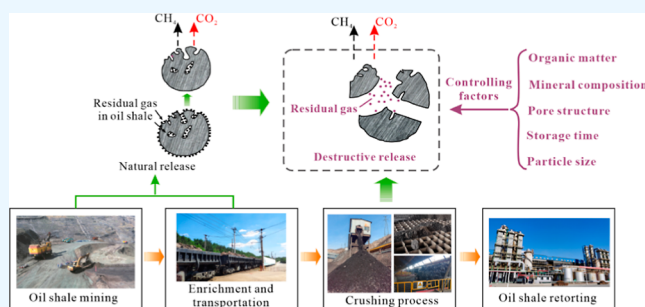
Read Online

ACCESS |

Metrics & More

Article Recommendations

**ABSTRACT:** Geological bodies are important sources of greenhouse gas (GHG) emissions. Organic-rich oil shale in sedimentary basins is a good gas source rock, the GHG in which will be released into the atmosphere during crushing to affect climate change. Quantitative calculations of GHG emissions during oil shale crushing were carried out on oil shales from the Yaojie (YJ) and Fushun (FS) mining areas in China. Organic geochemistry, X-ray diffraction, and pore structure analysis experiments, as well as the relationship between storage time and GHG emissions, were analyzed to investigate the main controlling factors of GHG release in different types of oil shales. The results showed that the CH<sub>4</sub> and CO<sub>2</sub> released from the YJ oil shale were 0.002–0.145 mL/g and 0.011–0.054 mL/g, respectively; the CH<sub>4</sub> and CO<sub>2</sub> released from the FS oil shale were 0.0001–0.0008 mL/g and 0.002–0.045 mL/g, respectively. Residual CH<sub>4</sub> release was closely related to total organic carbon (TOC) and maturity: the CH<sub>4</sub> released from the organic-rich and mature YJ oil shale was much higher than that of the FS oil shale, which is relatively organic-lean and immature. The control factors of the released CO<sub>2</sub> vary in different regions: CO<sub>2</sub> released from the YJ oil shale was somewhat affected by the TOC, while that released from the FS oil shale was mainly controlled by carbonate minerals and their contributing pores. The results of pore structure and organic maceral analyses indicated that both organic and inorganic pores of the YJ oil shale are occupied by asphaltenes, forming a key gas preservation mechanism of residual CH<sub>4</sub> and CO<sub>2</sub> as solutes dissolved in asphaltenes. In addition, CO<sub>2</sub> has a greater absorptive capacity than CH<sub>4</sub> and is therefore more difficult to release during the same crushing time. As oil shale is stored for longer periods, residual CH<sub>4</sub> will be preferentially released to the atmosphere, while residual CO<sub>2</sub> will be released in large quantities during crushing.



## 1. INTRODUCTION

Oil shale can be defined as a sedimentary rock containing various amounts of solid organic materials dispersedly bound in a mineral matrix.<sup>1</sup> The organic phase is usually of excellent economic and practical value, making oil shale a renewed research focus in the last several years.<sup>1–5</sup> In addition to obtaining shale oil and combustible gas through low-temperature retorting on the ground,<sup>6–9</sup> recent studies have suggested that oil shale is a fine gas source rock,<sup>10,11</sup> whose gas content can approach the lower limit of the Lewis shale in the San Juan Basin, United States.<sup>12</sup>

Unfortunately, according to the latest assessment report by the IPCC, coal, peat, and oil shale were the largest contributors to CO<sub>2</sub> emissions in the energy sector from 2015 to 2019.<sup>13</sup> Among them, oil shale's greenhouse gas (GHG) emission intensity was second only to lignite.<sup>14</sup> Furthermore, life-cycle GHG emission assessment believed that the GHG emission sources of oil shale were mainly from mining, transportation, and shale oil production.<sup>15–17</sup> A calculation of the gas emission from the oil shale overlying the coal seam in Guantun Coal

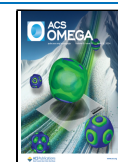
Mine showed that the gas content and relative gas emission of oil shale during the mining process were 0.09 and 0.22–0.4 m<sup>3</sup>/t, respectively.<sup>18</sup> Meanwhile, the methane emission sources have been detected recently by a shortwave airborne spectrographic imager from the oil shale open-pit mining area in the southeastern Junggar Basin.<sup>19</sup> Based on the above research, the GHG emissions caused by oil shale mining and destruction cannot be ignored. In addition, previous investigations on the factors affecting methane emissions in Green River oil shale suggested that methane content was directly related to yellow lamalginite content.<sup>20</sup> However, this type of methane was obtained by the natural desorption of oil shale rather than by including residual methane released after

Received: January 13, 2024

Revised: March 19, 2024

Accepted: March 22, 2024

Published: April 2, 2024



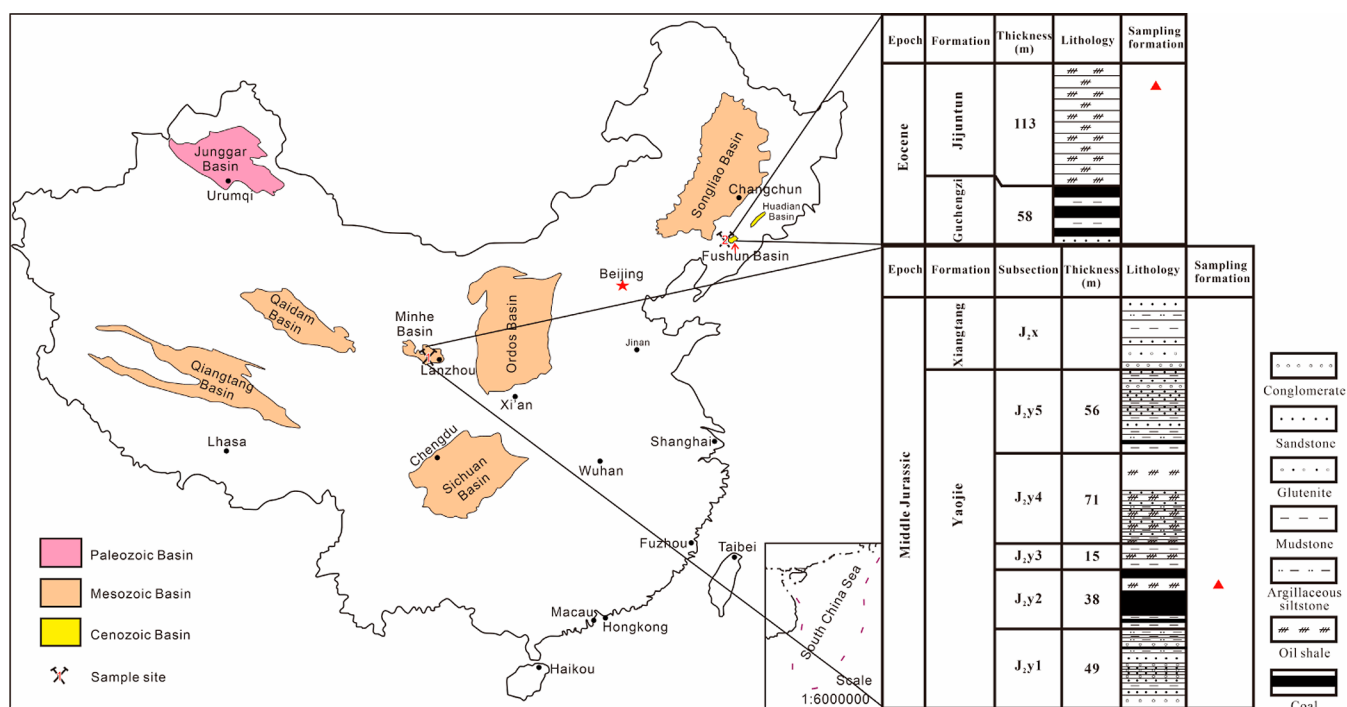


**Figure 1.** Sampling locations and stratigraphic histograms of the Middle Jurassic YJ Formation in the Minhe Basin and the Eocene Jijuntun Formation in the FS Basin [the sampling location map referenced with permission from Yu et al.,<sup>4</sup> copyright 2019 Elsevier Ltd.; the YJ Formation referenced with permission from Han et al.,<sup>34</sup> copyright 2019 Elsevier B.V.; and the Jijuntun Formation referenced with permission from Xu et al.,<sup>35</sup> copyright 2012 Editorial office of Journal of China University of Petroleum (Edition of Natural Science)].

destructive treatment. It is worth noting that large blocks of oil shale must be crushed and screened to meet the grain size requirements of the retort furnace before retorting. As a result, the residual gas molecules stored in closed pores that cannot escape under natural desorption conditions are released during the crushing process,<sup>21</sup> accompanied by the diffusion of GHG components. Nevertheless, most current studies focused on GHG emissions during oil shale retorting,<sup>22–24</sup> while few monitoring and in-depth studies were conducted on CH<sub>4</sub> and CO<sub>2</sub> emissions during crushing.

Residual gas is usually the gas released by crushing after the desorption of gas-bearing shale samples.<sup>25–28</sup> Although the residual gas yield is small, it is relatively stable and can be tested using rock samples that have been placed for a long time.<sup>29</sup> The residual gas characteristics of organic-rich shale and coal seams have been studied by many researchers.<sup>21,25,28,30,31</sup> The research on rock crushing gas of nine Barnett shales with different total organic carbon (TOC) contents and thermal maturity indicated that over 80% of the accumulated CH<sub>4</sub> was released from crushing coarse grains into fine grains,<sup>25</sup> and the decreases in the C<sub>1</sub>/CO<sub>2</sub> ratio with longer crushing time indicated that the CO<sub>2</sub> gas remained in the smaller pores. However, the absolute residual gas volumes obtained from Wufeng–Longmaxi shales with high thermal maturity and medium TOC contents in the northwest of the Hubei Province were in the range of 21–88 L/T and mainly CO<sub>2</sub> (60–97 vol %), while the CH<sub>4</sub> content was in proportion to carbonates.<sup>26</sup> Yang et al.<sup>31</sup> analyzed the relationship between moisture, ash, volatiles, and the residual gas in coal samples, and they found that the residual gas content was negatively correlated with the ash and internal water content in coal and positively correlated with the degree of coal metamorphism. These studies suggest that the differences in organic and

mineral components of shales, thermal maturity, and pore structure may all cause the differences in residual CH<sub>4</sub> and CO<sub>2</sub> contents released after crushing. But until now, there has been little quantitative research on residual CH<sub>4</sub> and CO<sub>2</sub> in oil shale. Quantitative analysis of CH<sub>4</sub> and CO<sub>2</sub> in residual gas from oil shale is critical to accurately assessing the GHG emission intensity during the crushing process.



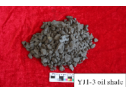


In this study, selected oil shale samples with different TOC contents and thermal maturity from two significant oil shale development and utilization areas were identified in China: the Fushun (FS) oil shale-bearing area in the Liaoning Province and the Yaojie (YJ) oil shale-bearing area in the Gansu Province. Using the analysis methods of geochemistry, mineralogy, and petrophysical properties, the GHG release characteristics in the oil shale residual gas obtained by the crushing method were studied. This study aims to (1) quantitatively calculate and compare the GHG content in the residual gas released after crushing of oil shale with different organic matter contents; (2) analyze the influence of oil shale composition and pore structure on the GHG release in the residual gas; and (3) discuss the impact mechanism of oil shale storage time and particle size on the differential release of different GHGs in residual gas. Our results are of great significance in quantifying the amount of residual GHG released from oil shale and elucidating its correlation with the geochemical and physical properties of oil shale.

## 2. MATERIALS AND METHODS

**2.1. Materials.** The YJ oil shale mining area in the Gansu Province is a typical demonstration area for the integrated utilization of oil shale. Commercially exploited oil shale was produced in the Middle Jurassic YJ Formation in the Minhe Basin (Figure 1), which was deposited in a lake-swamp

environment<sup>32</sup> and interbedded with coal and has an oil yield greater than 8%. Since the particle size of the raw material required by the YJ SJ-IV retorting furnace is 8–65 mm, large pieces of oil shale must be crushed to this particle size range before retorting. Therefore, we collected six blocks of oil shale with grain sizes larger than 65 mm; two cans each of oil shale with grain sizes of 8–65 mm and less than 8 mm for the first time at the YJ Oil Shale Comprehensive Utilization Co., Ltd. (YJ1); and three blocks of oil shale with grain sizes larger than 65 mm for the second time (YJ2). The color of the oil shale samples is mostly black to deep black (Table 1).

**Table 1. Basic Information on the Studied Oil Shale Samples**

Sample	Size (mm)	layer	Region	Sample photos
YJ1-1-1	>65			
YJ1-1-2				
YJ1-1-3				
YJ1-2-1	8-65	Middle Jurassic Yaojie Formation	Yaojie Haishiwan Coal Mine	
YJ1-2-2				
YJ1-3-1				
YJ1-3-2	<8			
YJ2-I	>65			
YJ2-II				
YJ2-III				
FS-I	>75	Palaeogene Eocene Jijuntun Formation	Fushun East Open-pit Mine	
FS-II				
FS-III				
FS-IV				

The FS oil shale mining area in the Liaoning Province is an important coal and oil shale industrial base in China with a development history of 30 years. The oil shale used for oil production by retorting was produced from the Paleogene

Eocene Jijuntun Formation in the FS Basin (Figure 1), which was deposited in the anoxic freshwater environment of a deep lake and located above the coal seam.<sup>33</sup> The oil yield of the ore-rich oil shale is 6–12%. The raw material particle size processed by the FS retort furnace is 12–75 mm. We collected four pieces of oil shale from the FS Shale Oil Plant with a particle size greater than 75 mm (FS), and the colors are gray-brown and gray-black (Table 1).

Among them, YJ1 oil shale samples were stored at room temperature for one year, and YJ2 and FS oil shale samples were stored for four months under the same conditions. In order to avoid errors caused by heterogeneity, each block YJ2 sample (YJ2-I, YJ2-II, and YJ2-III) and FS sample (FS-I, FS-II, FS-III, and FS-IV) bigger than 65 mm was divided into three parts for experiments. The basic information on the studied samples is listed in Table 1.

**2.2. Total Organic Carbon and Mineralogical Analysis.** TOC content was measured using a CS-344 analyzer after oil shale samples were ground to 80–100 mesh and soaked with 12.5% hydrochloric acid for 12 h to remove carbonates. The mineral component was measured with a Japanese Rigaku Ultima IV type X-ray diffraction analyzer with a scanning angle of 2–52° and a scanning speed of 3°/min after oil shale samples were ground to below 200 mesh.

**2.3. Vitrinite Reflectance (Ro) and Kerogen Maceral Analysis.** Vitrinite reflectance (Ro) was measured using the “Axio Scope. A1” Pol microscope and MSP200 instrument. The surface of the block sample crushed to about 2 cm was ground and polished, and then the polished sample was placed under a microscope for vitrinite detection. Each sample needs to be tested at 20 points, and then the average value is taken to obtain Ro.

Kerogen maceral analysis used the traditional HCl–HF acidolysis method. Fresh samples of 20–50 g were selected and crushed to about 2 mm particles and placed in a 500 mL beaker. The carbonate minerals in the samples were first removed with 10% HCl at room temperature with sufficient agitation, and then 70% HF was used to remove the siliceous rocks in the samples after repeated washing with distilled water

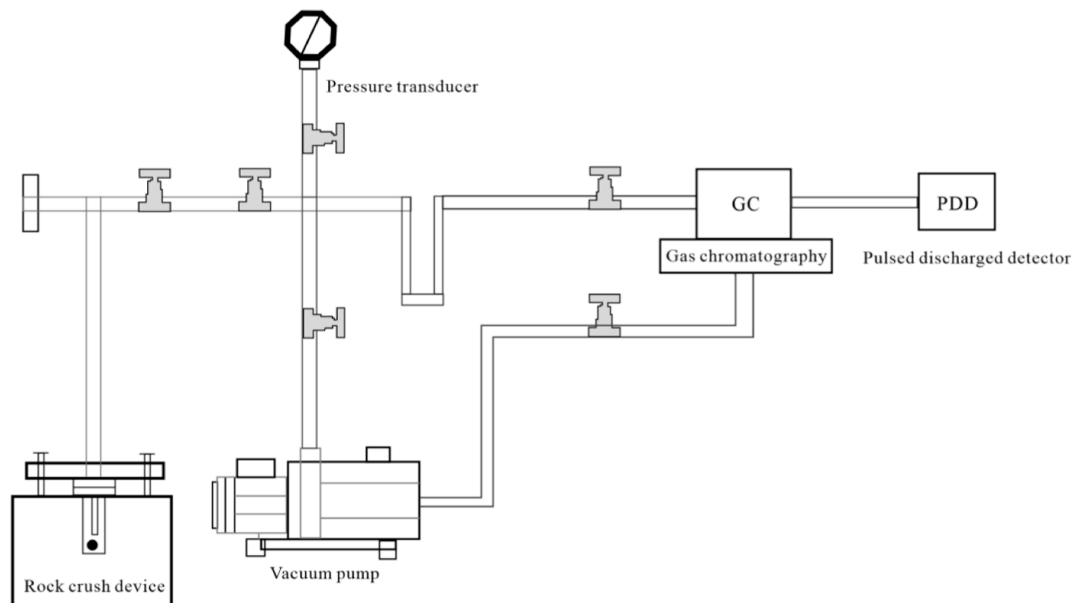


**Figure 2.** Schematic diagram of the rock degassing device and chemical composition analysis of residual gas.

Table 2. Geochemical Parameters and Mineralogical Compositions of the Studied Oil Shale Samples<sup>a</sup>

sample	TOC (wt %)	Ro (%)	quartz	feldspar	carbonate	pyrite	anatase	total clay
YJ1-1-1	21.78	0.98	44.6	0.8	0	2.5	1.5	50.6
YJ1-1-2	31.66	1.01	44.1	0.9	5.0	3.2	1.4	45.4
YJ1-1-3	23.76	0.97	42.1	1.8	5.8	1.5	1.4	47.4
YJ1-2-1	16.67	0.95	43.6	0.7	14.1	5.4	1.0	35.2
YJ1-2-2	29.88		47.3	2.1	6.4	6.0	1.1	36.5
YJ1-3-1	21.52		47.0	1.1	11.8	2.2	1.5	36.4
YJ1-3-2	19.97	1.01	53.2	1.9	5.2	1.8	1.9	36.0
YJ2-1	30.69	1.15	59.0	1.1	7.6	5.3	0	27.0
YJ2-2	31.00	1.25	53.9	1.0	0.8	3.2	0	41.1
YJ2-3	30.86	1.16	54.4	1.8	4.1	4.3	1.5	33.9
YJ2-4	27.06	1.21	59.0	2.7	6.7	0	0.9	30.7
YJ2-5	30.69	1.20	56.9	0.9	7.8	3.1	0.8	30.5
YJ2-6	29.01	1.24	56.8	2.7	7.9	2.1	0.9	29.6
YJ2-7	28.19	1.03	52.3	5.0	0.5	3.3	1.2	37.7
YJ2-8	27.46	1.18	67.4	2.9	2.5	3.3	0.8	23.1
YJ2-9	29.16	1.10	68.0	1.1	1.5	2.8	0.7	25.9
FS-1	8.02	0.23	37.1	4.7	6.6	1.3	0	50.3
FS-2	8.19	0.25	34.2	4.9	8.5	1.4	2.7	48.3
FS-3	7.84	0.27	34.0	4.8	5.9	0.6	2.8	51.9
FS-4	4.25	0.26	24.1	2.8	23.1	2.5	3.2	44.3
FS-5	4.13	0.33	24.6	2.5	20.8	1.9	2.3	47.9
FS-6	4.38	0.33	27.3	3.6	9.7	1.3	3.7	54.4
FS-7	8.37	0.25	37.3	5.6	5.0	0.8	4.0	47.3
FS-8	8.37	0.20	34.5	4.8	5.7	1.4	3.3	50.3
FS-10	8.00	0.29	31.6	3.7	6.8	2.3	2.6	53.0
FS-11	8.36	0.29	33.3	5.0	5.2	1.9	3.2	51.4
FS-12	8.43	0.28	32.5	4.0	5.6	1.2	2.9	53.8

<sup>a</sup>Note: The unit of mineralogical compositions is mass percentage (wt %).

to neutrality and then washed repeatedly with distilled water to neutrality and centrifuged. The acidolysis residues obtained were sectioned, and the macerals were identified, counted, and photographed under a microscope. The microscope model is a Zeiss AXO 40.

**2.4. Low-Pressure N<sub>2</sub> Adsorption Analysis.** Low-pressure N<sub>2</sub> adsorption was measured on a Micromeritics ASAP 2020 HD88 surface area analyzer. About 0.3 g of oil shale samples was powdered into 60–80 mesh and automatically degassed at 110 °C for 12 h under vacuum to remove adsorbed moisture and volatile substances.<sup>36</sup> The degassed sample was exposed to N<sub>2</sub> at a temperature of −196 °C within a range of precisely controlled gas pressures. The N<sub>2</sub> adsorption volumes were measured in the relative equilibrium adsorption pressure (P/P<sub>0</sub>) range from 0.0001 to 0.995, where P<sub>0</sub> is the saturated vapor pressure of N<sub>2</sub> under laboratory conditions and P is the actual gas pressure in the sample chamber. All samples did not remove soluble organic matter. The pore structure parameters generally refer to pore volume, surface area, and pore size distribution (PSD). The Brunauer–Emmett–Teller (BET) model was widely used to characterize the surface area of the porous adsorbent.<sup>34,36,37</sup> In this study, the surface area of the oil shale samples was obtained using the BET method. The pore volume and varied range of PSDs were acquired using the density functional theory (DFT) model, which can more accurately analyze narrow mesopores but also reliably determine the PSDs in the ranges of meso- to macropore dimensions.<sup>38,39</sup> In the calculation of pore structure parameters, the data were used from the isotherms' adsorption branches.<sup>40</sup> Twelve valuable experimental data points were

selected from the N<sub>2</sub> adsorption data of 27 samples to characterize the pore structure characteristics of oil shale.

**2.5. Acquisition and Quantitative Calculation of Residual Gas.** Residual gas in oil shale was acquired and analyzed utilizing an assembled apparatus of a high-vacuum electromagnetic crusher coupled with gas chromatography (GC) with a pulsed discharge detector (Figure 2). Quantitative rock samples were degassed by high-vacuum electromagnetic crushing. The gas pressure before and after crushing was monitored by a thin-film vacuum gauge, assuming that the temperature remained constant before and after the crushing. Then, the gas entered the GC sample loop, where the chemical composition and relative amount of residual gas released were detected through a highly sensitive GC system.<sup>41</sup> The total residual gas volume released in the standard state was obtained after conversion using the ideal gas state equation ( $pV = nRT$ ). The absolute volumes of CH<sub>4</sub> and CO<sub>2</sub> in the residual gas were calculated by multiplying the total residual gas volume by the relative percentages of CH<sub>4</sub> and CO<sub>2</sub>.

Approximately 2–5 g of gravel-size oil shale samples was loaded into the specially fitted stainless-steel sample-crushing tank, and the lid fitted with an O-ring seal was screwed. The tank was evacuated, and a pipeline was connected to the GC with a vacuum pump, and then the valve was closed until the pressure stabilized below 20 Pa. Samples were crushed for 30–40 s until most residual gas was released. The valve connected to the pressure sensor was opened, and the gas pressure was recorded. Then, the inlet valve of the GC was opened, and the gas entered the GC-PDD from the crusher for gas composition analysis. The GC-9560-PDD was equipped with a pneumatic ten-way valve, a six-way valve, and two chromatographic

Table 3. Kerogen Organic Macerals of the Studied Oil Shale Samples

sample	sapropelite (%)			exinite (%)							vitrinite (%)	inertinite (%)	organic matter type
	algite	amorphous	total	resinite	suberinite	cutinite	sporinite	amorphous	Benthic algae	total			
FS-1	1.0	63.1	64.1	1.0	11.7	3.9	3.9	0.0	4.9	25.2	10.7	0.0	II <sub>1</sub>
FS-5	5.1	45.5	50.5	0.0	6.1	2.0	8.1	13.1	5.1	34.3	14.1	1.0	II <sub>1</sub>
FS-12	0.0	0.0	0.0	1.0	11.9	3.0	3.0	55.4	10.9	85.1	12.9	2.0	II <sub>1</sub>
YJ1-1-1	0.0	0.0	0.0	0.0	6.7	3.8	0.0	0.0	30.5	41.0	53.3	5.7	II <sub>2</sub>
YJ1-1-2	6.1	0.0	6.1	0.0	14.3	0.0	0.0	1.0	49.0	64.3	28.6	1.0	II <sub>2</sub>
YJ1-2-1	2.0	0.0	2.0	1.0	23.5	1.0	1.0	44.1	12.7	83.3	12.7	2.0	II <sub>1</sub>
YJ1-3-2	3.1	0.0	3.1	2.1	32.3	2.1	1.0	13.5	4.2	55.2	39.6	2.1	II <sub>2</sub>
YJ2-8	1.0	0.0	1.0	1.0	37.1	2.1	0.0	2.1	14.4	56.7	41.2	1.0	II <sub>2</sub>
YJ2-9	0.0	0.0	0.0	0.0	34.7	0.0	0.0	4.1	12.2	51.0	45.9	3.1	II <sub>2</sub>

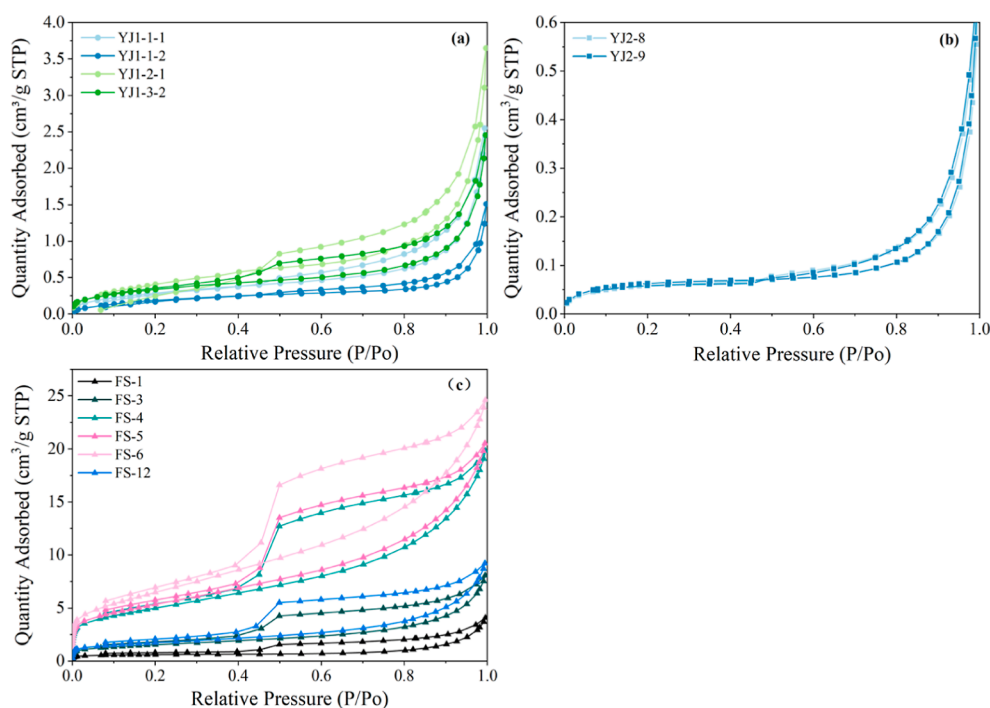


**Figure 3.** Low-pressure  $N_2$  adsorption isotherms of oil shale samples: (a) YJ1 oil shale; (b) YJ2 oil shale; (c) FS oil shale;  $P$ : actual gas pressure;  $P_0$ : saturated vapor pressure of  $N_2$ ; STP: standard ambient temperature and pressure (25 °C and 100 kPa).

columns. The Porapak Q chromatographic columns (2 m  $\times$  1/16 in.) were installed in a column box with a precolumn pressure of 0.4 MPa; the other is a 5 Å molecular sieve chromatographic column (0.5 m  $\times$  1/8 in.) installed in an auxiliary furnace, with a precolumn pressure of 0.4 MPa, a constant temperature of 60 °C, and a detector temperature of 250 °C. The heating procedure of GC was first held at 110 °C for 5 min and then heated to 240 °C at 10 °C/min, where it was held for 12 min.

### 3. RESULTS

**3.1. Organic and Inorganic Composition.** The geochemical and mineralogical characteristics of YJ and FS oil shale samples are given in Table 2. The TOC contents of YJ oil shales range from 16.67 wt % to 31.66 wt %, with an average value of 26.83 wt %. The vitrinite reflectance ( $R_o$ ) ranges between 0.95 and 1.25%, with an average value of 1.10%. It indicates the high organic matter content of the YJ oil shale, which is currently within the oil window and even beginning to generate wet gas.<sup>42</sup>

The TOC values of FS oil shales are 4.13–8.43 wt %, with a mean value of 7.22 wt %. The  $R_o$  values range from 0.20 to 0.33%, with a mean value of 0.27%. The FS oil shale is significantly lower in organic matter than the YJ oil shale and is in the immature stage.

It can be seen from Table 3 that the kerogen organic macerals of oil shale samples are composed of sapropelite, exinite, vitrinite, and inertinite. The principal organic components of FS oil shales are sapropelite with an average content of 50.5%, containing a large amount of sapropelitic amorphous bodies; the average contents of exinite, vitrinite, and inertinite are 38.3, 10.4, and 0.75%, respectively. The primary organic components of YJ oil shales are exinite with an average content of 58.6%, in which suberinite is generally high; the average contents of sapropelite, vitrinite, and inertinite are 2.0, 36.9, and 2.5%, respectively.

The dominant mineral components of YJ oil shales are quartz, clays, and carbonate, with contents of 42.1–68.0%, 23.1–50.6%, and 0–14.1%, respectively (Table 2), followed by

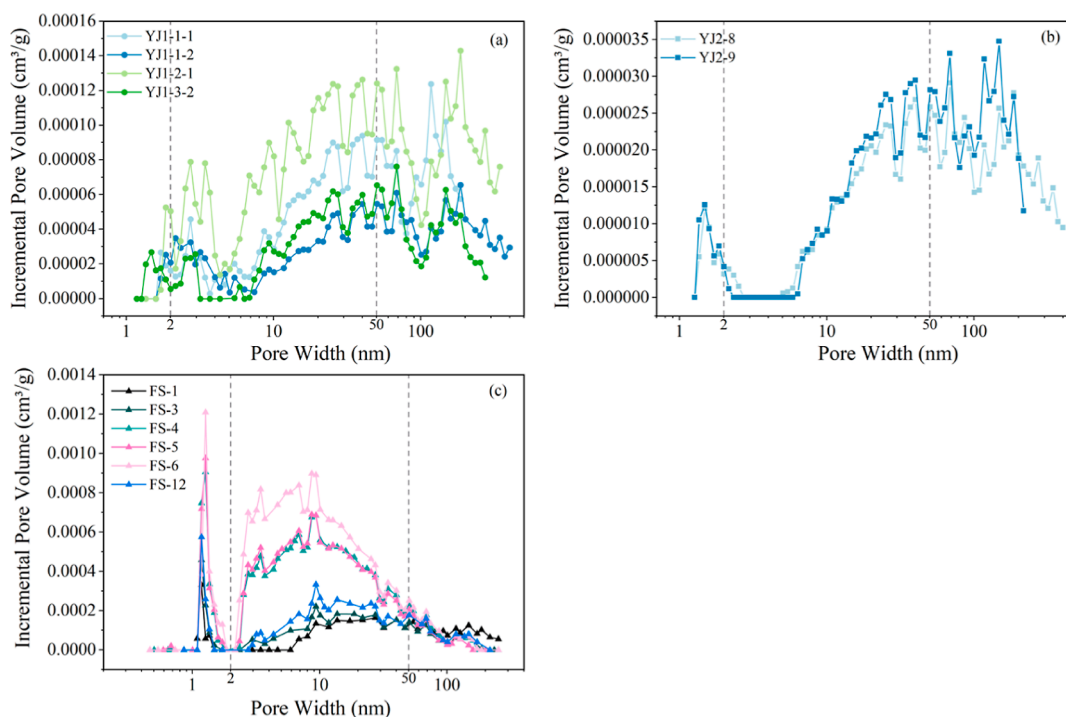


**Figure 4.** PSD of oil shale samples calculated by DFT methods: (a) YJ1 oil shale; (b) YJ2 oil shale; and (c) FS oil shale.

pyrite, feldspar, and anatase, with contents ranging from 0 to 6.0%, 0.7–5.0%, and 0–1.9%, respectively.

The mineral composition of the FS oil shales is also mainly clays, quartz, and carbonate, with contents of 44.3–54.4%, 24.1–37.3%, and 5.0–23.1%, respectively; the contents of feldspar, anatase, and pyrite are relatively low, which are 2.5–5.0%, 0–4.0%, and 0.6–2.5%, respectively. Clay and carbonate minerals are higher than those of the YJ oil shale, while the quartz content is lower than that of the YJ oil shale.

**3.2. Pore Structure Characteristics.** **3.2.1. Low-Pressure  $N_2$  Adsorption Isotherms.** The low-pressure  $N_2$  adsorption isotherms of YJ and FS oil shale samples are shown in Figure 3. According to the classification of adsorption isotherms given by IUPAC (International Union of Pure and Applied Chemistry),<sup>37,43</sup> the type II isotherms correspond to the studied samples, which indicated that micropores ( $r < 2$  nm) and mesopores ( $2 \text{ nm} < r < 50$  nm) are predominant.<sup>44</sup> The shape of such isotherms results from unrestricted monolayer-multilayer adsorption up to high  $P/P_0$ .<sup>43</sup> The steep curve rises where  $P/P_0 > 0.8$  in all samples because of capillary condensation,<sup>45</sup> implying that the extensive adsorbate filled into the mesopores and macropores.

The FS oil shales show steeper isotherms in the pressure range of  $P/P_0 < 0.1$ , indicating that there is a specific surface area in the micropore range (Figure 3c). The shape of the hysteresis loop of FS oil shales is similar to the H4 type. According to the classification of pore types provided by Thommes,<sup>43</sup> the pores in the FS oil shale can be recognized as the narrow slit-type.<sup>34</sup>

On the contrary, the YJ1 and YJ2 oil shales display less  $N_2$  adsorption in the pressure range of  $P/P_0 < 0.1$  and hence less microporosity (Figure 3a,b). The YJ1 and YJ2 oil shales show a type H3 hysteresis loop (Figure 3a,b), suggesting that plate-like particles induce slit-shaped pores.<sup>37</sup>

**3.2.2. Pore Size Distribution.** The PSDs of the oil shale samples are displayed in Figure 4. The incremental pore

volumes related to PSD were acquired by the DFT analysis method. Based on IUPAC's pore size classification, pores with a width of less than 2 nm are micropores, those between 2 and 50 nm are mesopores, and those over 50 nm are macropores.<sup>37</sup> From the PSD curves of the YJ1 oil shale, it can be observed that the pore sizes are mainly mesopores of 2–4 nm and 6–50 nm and macropores of 50–80 nm and 100–200 nm. The micropores are relatively small (Figure 4a). In particular, YJ2 oil shales mainly developed mesopores of 15–50 nm and macropores of 50–200 nm, while micropores of less than 2 nm are almost undeveloped (Figure 4b). And the corresponding incremental pore volumes are much smaller than those of YJ1 oil shales. However, the PSD of the FS oil shale is focused on micropores and mesopores (2–20 nm), but macropores are relatively undeveloped (Figure 4c).

**3.2.3. Surface Area and Pore Volume.** The data of pore structure parameters of YJ and FS oil shale samples are listed in Table 4 and plotted in Figure 5.

Table 4 shows that the total pore volume of YJ1 oil shales ranges from 2.04 to 5.51  $\mu\text{L/g}$ , with an average value of 3.23  $\mu\text{L/g}$ . Among them, the volumes of micropores, mesopores, and macropores are 0.04–0.09  $\mu\text{L/g}$ , 0.88–3.11  $\mu\text{L/g}$ , and 0.92–2.34  $\mu\text{L/g}$ , with an average proportion of 4.23, 60.23, and 35.54%, respectively (Figure 5). The YJ2 oil shale has the smallest total pore volume of 1.01  $\mu\text{L/g}$  among the studied oil shale samples. Specifically, the micropore volume is 0.04–0.05  $\mu\text{L/g}$ , which is comparable to that of the YJ1 oil shale, and the mesopore and macropore volumes are 0.44–0.48  $\mu\text{L/g}$  and 0.49–0.53  $\mu\text{L/g}$ , respectively, which are significantly smaller than those of the YJ1 oil shale. The average percentages of the three pore volumes are 8.36, 52.23, and 39.42%, respectively.

Nevertheless, the total pore volume of FS oil shales is the largest in the studied samples, ranging from 3.06 to 20.98  $\mu\text{L/g}$ , with an average value of 9.98  $\mu\text{L/g}$ . Compared with YJ oil shales, the volume of micropores and mesopores increases, but the volume of macropores decreases, which are 0–2.50  $\mu\text{L/g}$ ,

**Table 4. Pore Structure Parameters of the Studied Samples<sup>a</sup>**

sample	$S_{\text{BET}}$ ( $\text{m}^2/\text{g}$ )	$V_{\text{DFT}}$ ( $\mu\text{L}/\text{g}$ )	micropores ( $\mu\text{L}/\text{g}$ )	mesopores ( $\mu\text{L}/\text{g}$ )	macropores ( $\mu\text{L}/\text{g}$ )
YJ1-1-1	1.11	3.23	0.05	1.81	1.37
YJ1-1-2	0.75	2.04	0.04	0.88	1.12
YJ1-2-1	1.64	5.51	0.06	3.11	2.34
YJ1-3-2	1.25	2.14	0.09	1.13	0.92
YJ2-8	0.20	1.01	0.04	0.44	0.53
YJ2-9	0.21	1.01	0.05	0.48	0.49
FS-1	1.94	3.18	0.52	1.37	1.29
FS-3	5.40	3.59	0.80	2.14	0.65
FS-4	17.74	16.67	2.23	13.06	1.38
FS-5	19.05	16.67	2.34	13.20	1.13
FS-6	23.67	20.98	2.50	16.98	1.50
FS-12	6.02	5.70	0.94	3.83	0.93

<sup>a</sup> $S_{\text{BET}}$ : BET special surface area;  $V_{\text{DFT}}$ : DFT total pore volume.

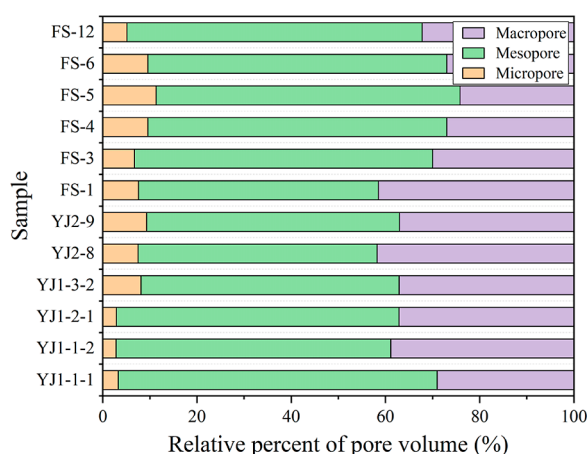


**Figure 5.** Relative percentage of pore volumes of micropores, mesopores, and macropores of the studied samples.

1.31–16.98  $\mu\text{L}/\text{g}$ , and 0.65–1.75  $\mu\text{L}/\text{g}$ , accounting for 7.09, 59.13, and 33.77% on average, respectively (Figure 5).

Micropores mainly provide the surface area. Overall, the FS oil shales possess a higher surface area than the YJ oil shales, which is 1.26–23.67  $\text{m}^2/\text{g}$  (average of 10.73  $\text{m}^2/\text{g}$ ) (Table 4). In comparison, the YJ oil shales have a low surface area, ranging from 0.2 to 1.64  $\text{m}^2/\text{g}$  (average of 0.86  $\text{m}^2/\text{g}$ ), corresponding to their low micropore volume.

**3.3. Total Residual Gas.** The gas composition (normalized to 100%) and absolute volume of the total residual gas released from oil shale after crushing are given in Table 5. The absolute residual gas yield in YJ oil shales is 0.17–0.42  $\text{mL}/\text{g}$ , and the gas is basically composed of  $\text{C}_1$ ,  $\text{C}_2$ , and  $\text{C}_3$  gaseous hydrocarbons ( $\text{C}_1 + \text{C}_2 + \text{C}_3$  almost accounts for more than 50%) and  $\text{CO}_2$ ,  $\text{CO}$ ,  $\text{N}_2$ ,  $\text{H}_2$ ,  $\text{O}_2$ , and Ar.

The absolute residual gas yield in FS oil shales is 0.05–0.19  $\text{mL}/\text{g}$ , which is lower than that in YJ oil shales, and the gas is mainly composed of nonhydrocarbon gas, but the total proportion of  $\text{C}_1$ – $\text{C}_3$  is less than 1.1%. Ethylene is the only detected component of unsaturated gaseous hydrocarbons, but the concentration is extremely low.

**3.4. Absolute Amounts of  $\text{CH}_4$  and  $\text{CO}_2$  in Residual Gas.** The GHG components in the oil shale residual gas are  $\text{CH}_4$  and  $\text{CO}_2$ . The calculated absolute amounts of  $\text{CH}_4$  in residual gas from YJ1, YJ2, and FS oil shales are 0.002–0.030  $\text{mL}/\text{g}$ , 0.031–0.145  $\text{mL}/\text{g}$ , and 0.0001–0.0008  $\text{mL}/\text{g}$ ,

respectively (Table 6). The residual  $\text{CH}_4$  released from the YJ oil shale is two orders higher than that from the FS oil shale. The absolute amounts of residual  $\text{CO}_2$  released from YJ1, YJ2, and FS oil shales are 0.011–0.034  $\text{mL}/\text{g}$ , 0.017–0.054  $\text{mL}/\text{g}$ , and 0.002–0.045  $\text{mL}/\text{g}$ , respectively (Table 6). The residual  $\text{CO}_2$  content in the FS oil shale is slightly less than that in the YJ oil shale.

## 4. DISCUSSION

**4.1. Effect of Oil Shale Composition on  $\text{CH}_4$  and  $\text{CO}_2$  Contents in Residual Gas.** The organic matter content and mineral components were crucial factors influencing shale gas potential.<sup>46–49</sup> For the purpose of researching how the composition of oil shale affects the absolute content of  $\text{CH}_4$  and  $\text{CO}_2$  in residual gas, we discuss the effect of organic matter and inorganic mineral components on the content of residual  $\text{CH}_4$  and  $\text{CO}_2$  in YJ and FS oil shales, respectively.

**4.1.1. Effect of Organic Matter on Residual  $\text{CH}_4$  and  $\text{CO}_2$ .** The TOC was argued to be one of the most critical elements controlling the pore structure and gas storage capacity in organic-rich shales. For example, the micro- and mesoporous surface areas of the Lower Cretaceous gas shales in northeastern British Columbia increase with TOC content, and the micropore volume increases with maturity for all kerogen types.<sup>46</sup> However, some studies found that the large methane adsorption capacity in the organic-rich shale was independent of surface area, and the influence of TOC on micropores was not apparent.<sup>49</sup> The following sections comprehensively discuss the impact of organic matter abundance, type, and thermal maturity on the absolute yield of residual  $\text{CH}_4$  and  $\text{CO}_2$  released by crushing.

It is first necessary to determine the development of organic matter pores in the oil shale samples before the effect of organic matter on residual  $\text{CH}_4$  and  $\text{CO}_2$ . As shown in Figure 6, the surface area and total pore volume of YJ and FS oil shales presented a clear negative correlation with the TOC content. This suggests that organic matter is not a major contributor to oil shale pore space.

The surface area and pore volume of the YJ oil shale are significantly lower than those of the FS oil shale. It indicates that the pores of the YJ oil shale are hardly developed or filled. This was also illustrated by the fact that no organic pores have been observed in the FE-SEM examination conducted on YJ Formation oil shales.<sup>34</sup> In a study that compared the changes in pore structure before and after the extraction of organic matter in shales of the Upper Triassic Yanchang Formation in the Ordos Basin, the author found that the occupation and blockage of shale pores by extractable organic matter were one of the reasons for the negative correlation between TOC and micropore volume<sup>36</sup> and stated that pores with small diameters would be preferentially occupied. The same case occurred in the shales of the Qingshankou Formation in the Songliao Basin.<sup>50</sup> In our work, the YJ oil shales are organically richer than FS oil shales and have entered the oil window (Table 2), so we reasonably believe that the reason the organic pores are undeveloped is that the pores were filled with asphaltene generated by the thermal evolution of organic matter.

Strangely, there is still a positive linear correlation between the TOC and the absolute volume of residual  $\text{CH}_4$  and  $\text{CO}_2$  released from YJ oil shales (Figure 7), although organic pores were occupied. Such findings imply that the preservation of residual  $\text{CH}_4$  and  $\text{CO}_2$  in YJ oil shales probably cannot be simply explained as surface adsorption. Furthermore, a study

**Table 5. Chemical Components and Absolute Volume of Residual Gas Released from Oil Shale Samples after Crushing**

sample	CH <sub>4</sub> (%)	C <sub>2</sub> H <sub>6</sub> (%)	C <sub>3</sub> H <sub>8</sub> (%)	C <sub>2</sub> H <sub>4</sub> (%)	CO <sub>2</sub> (%)	CO (%)	N <sub>2</sub> (%)	H <sub>2</sub> (%)	O <sub>2</sub> + Ar (%)	absolute amount (mL/g)
YJ1-1-1	8.28	20.38	38.84	0.03	9.44	0.04	13.39	8.77	0.84	0.36
YJ1-1-2	0.67	18.43	45.69	0.05	8.24	0.08	18.32	6.86	1.67	0.34
YJ1-1-3	3.90	14.11	30.80	0.03	6.74	0.03	17.39	26.00	1.00	0.24
YJ1-2-1	5.60	16.82	25.37	0.03	3.73	0.04	17.02	30.57	0.82	0.28
YJ1-2-2	0.94	17.88	32.57	0.07	8.33	0.06	18.12	20.84	1.20	0.30
YJ1-3-1	2.09	14.40	30.44	0.05	11.71	0.06	19.06	21.18	1.01	0.27
YJ1-3-2	1.19	7.74	17.24	0.06	19.81	0.05	17.25	35.83	0.83	0.17
YJ2-1	15.14	24.84	12.71	0.07	13.13	0.11	24.79	6.32	2.87	0.21
YJ2-2	23.04	25.26	8.92	0.05	9.01	0.08	25.66	5.00	2.98	0.19
YJ2-3	34.47	23.72	6.92	0.05	9.01	0.06	18.19	5.88	1.71	0.42
YJ2-4	10.58	20.57	12.81	0.07	12.18	0.10	28.82	11.26	3.60	0.32
YJ2-5	13.13	23.54	16.61	0.05	13.43	0.09	21.35	9.44	2.36	0.40
YJ2-6	12.92	19.49	11.36	0.04	8.68	0.02	13.71	33.30	0.47	0.22
YJ2-7	43.06	14.86	7.70	0.02	9.11	0.02	12.68	11.84	0.70	0.31
YJ2-8	27.71	19.69	11.87	0.05	9.90	0.04	16.19	13.56	1.00	0.34
YJ2-9	39.62	16.05	9.41	0.04	8.72	0.03	13.72	11.48	0.93	0.35
FS-1	0.62	0.04	0	0.08	23.69	0.37	41.90	31.09	2.20	0.13
FS-2	0.83	0.05	0	0.09	15.08	0.24	35.61	47.39	0.71	0.09
FS-3	0.25	0	0	0	56.34	0.29	10.33	32.42	0.38	0.09
FS-4	1.04	0.04	0	0.06	66.59	0.30	0.22	31.72	0.03	0.06
FS-5	0.96	0.05	0	0.12	66.94	0.46	0.22	31.22	0.02	0.07
FS-6	0.64	0.03	0	0.08	52.32	0.33	14.29	29.12	3.20	0.07
FS-7	0.21	0	0	0.03	6.64	0.21	70.36	10.27	12.29	0.08
FS-8	0.33	0	0	0.06	14.93	0.37	64.5	11.37	8.43	0.08
FS-10	0.04	0	0	0	81.93	0.24	12.56	4.71	0.52	0.08
FS-11	0.13	0	0	0.02	2.47	0.11	74.08	8.43	14.77	0.09
FS-12	0.77	0	0	0.08	16.76	0.53	47.97	32.7	1.19	0.05

**Table 6. Absolute Volumes of CH<sub>4</sub> and CO<sub>2</sub> in Residual Gas Released from the Oil Shale Samples**

sample	absolute gas amounts (mL/g)	
	CH <sub>4</sub>	CO <sub>2</sub>
YJ1-1-1	0.030	0.034
YJ1-1-2	0.002	0.028
YJ1-1-3	0.009	0.016
YJ1-2-1	0.016	0.011
YJ1-2-2	0.003	0.025
YJ1-3-1	0.006	0.032
YJ1-3-2	0.002	0.034
YJ2-1	0.031	0.027
YJ2-2	0.043	0.017
YJ2-3	0.145	0.038
YJ2-4	0.034	0.039
YJ2-5	0.053	0.054
YJ2-6	0.028	0.019
YJ2-7	0.134	0.028
YJ2-8	0.094	0.034
YJ2-9	0.140	0.031
FS-1	0.0008	0.031
FS-2	0.0008	0.014
FS-3	0.0006	0.017
FS-4	0.0007	0.043
FS-5	0.0006	0.045
FS-6	0.0004	0.036
FS-7	0.0002	0.005
FS-8	0.0003	0.012
FS-10	0.0004	0.018
FS-11	0.0001	0.002
FS-12	0.0004	0.008

on gas sorption of clays and oil shales showed that oil shale with lower surface areas adsorbed much more hydrocarbon gases than the clays with higher surface areas, implying other retention mechanisms, such as absorption.<sup>51</sup> Moreover, it has been proven that matrix bituminite can dissolve CH<sub>4</sub> and CO<sub>2</sub>.<sup>49,52</sup> Moreover, the exsudatinite was generated at the expense of exinites, formed only in the oil window, and confined to humic facies.<sup>53</sup> Our kerogen maceral analysis of oil shale samples indicated that YJ oil shales possess type II<sub>2</sub> organic matter, in which exinites account for a considerable percentage (Table 3, Figure 8), and have matured (average Ro is 1.10%) enough to produce a certain amount of bituminite. Therefore, significant quantities of residual CH<sub>4</sub> and CO<sub>2</sub> are reserved within YJ oil shales, despite a small surface area and total pore volumes, signifying the likelihood of CH<sub>4</sub> and CO<sub>2</sub> being solubilized within the matrix bituminite (analogous to solute gases within bitumen). CH<sub>4</sub> and CO<sub>2</sub> were released from the matrix asphaltenes due to the pressure release (the experimental sample was placed in a vacuum) and a slight increase in temperature during the crushing process.

On the other hand, the research of Svrcek showed that the solubility of CO<sub>2</sub> in bitumen was more excellent than that of CH<sub>4</sub>.<sup>52</sup> Furthermore, the sorption capacity of CO<sub>2</sub> was twice that of CH<sub>4</sub> for low-rank coals, which was caused by the more significant amounts of oxygen-containing functional groups,<sup>54</sup> and the type I kerogen had the characteristic of generally low oxygen-containing functional groups compared to type III. According to the fact that the type II<sub>2</sub> organic matter in the YJ oil shale possesses a relatively higher O/C ratio than that of the type II<sub>1</sub> organic matter in the FS oil shale in this study due to the existence of more oxygen-containing functional groups,<sup>42</sup> the bituminite evolved from the type II<sub>2</sub> organic matter absorbs



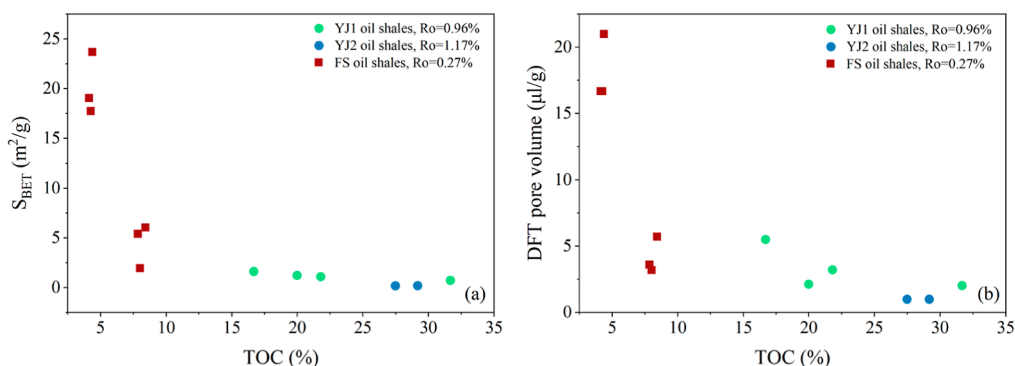


**Figure 6.** Relationships between TOC contents and (a) specific surface area and (b) pore volume of oil shale samples.

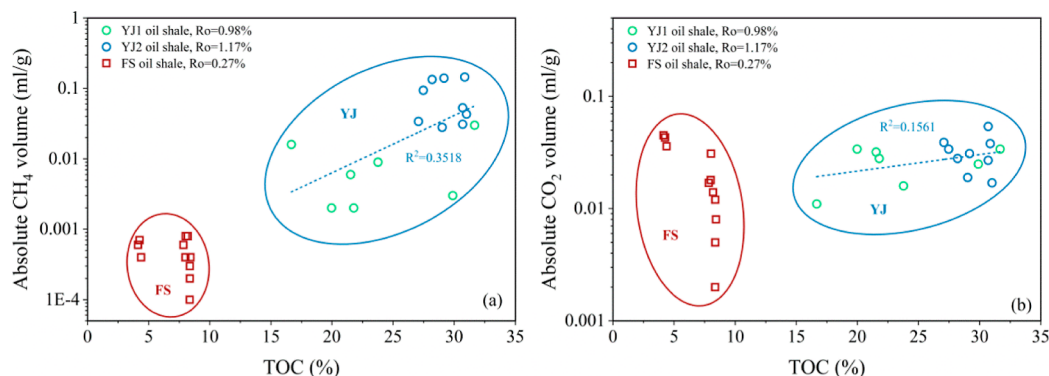


**Figure 7.** Relationships between TOC contents and absolute CH<sub>4</sub> (a) and CO<sub>2</sub> (b) volumes in the residual gas of oil shale samples.

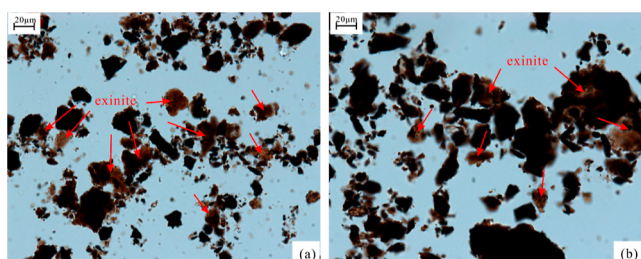


**Figure 8.** Kerogen maceral images in YJ oil shales under transmitted light: (a) YJ1-3-2; (b) YJ2-8.

CO<sub>2</sub> more strongly compared to CH<sub>4</sub>. Second, the gas release characteristics of the organic-rich shale at different crushing times have proven that as the crushing time is longer, the CH<sub>4</sub>/CO<sub>2</sub> ratio decreases, indicating a progressively greater release of CO<sub>2</sub>-rich gas.<sup>25</sup> This means that CO<sub>2</sub> is less easily released than CH<sub>4</sub> within a crushing time of 60 s. It explains well that the correlation between TOC and residual CH<sub>4</sub> ( $R^2 = 0.3518$ ) is stronger than CO<sub>2</sub> ( $R^2 = 0.1561$ ) (Figure 7) within 30–40 s of crushing time in this study.

For the FS oil shale, the TOC content is relatively low and immature (Table 2), which results in organic pores that have

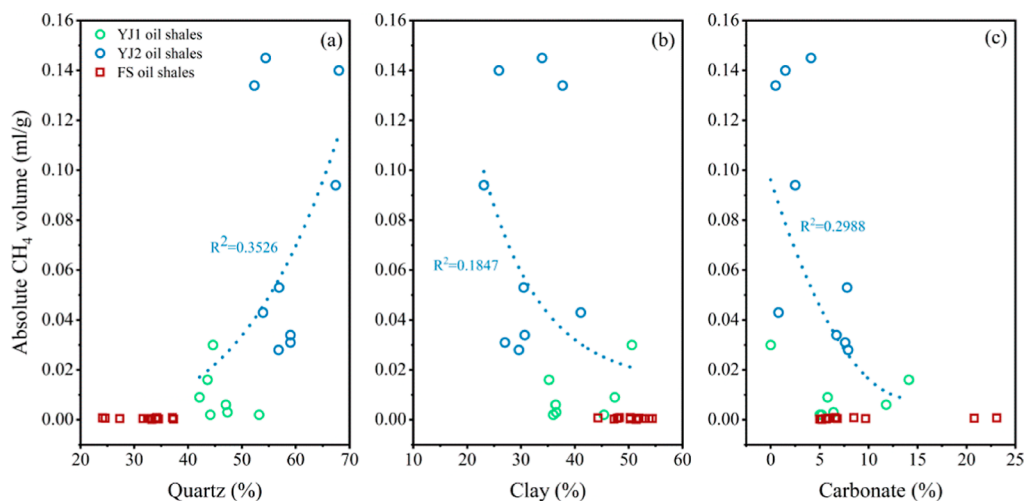


**Figure 9.** Relationships between the absolute CH<sub>4</sub> volume in residual gas and (a) quartz, (b) clay, and (c) carbonate content of the studied samples.

not yet formed. Other researchers have also not found organic pores in the FS oil shale.<sup>55</sup> This leads to a negative correlation between the TOC and pore structure in the FS oil shale (Figure 6). It is because of the immature organic matter and the preference of the organic matter type for oil production that the residual CH<sub>4</sub> release from the FS oil shale after crushing is extremely low and does not correlate significantly with the TOC (Figure 7a). However, a decreasing trend of residual CO<sub>2</sub> volume with the TOC was observed in FS oil shales (Figure 7b). It indicates that TOC is not the main controlling factor of residual CO<sub>2</sub> content in the FS oil shale. The residual CO<sub>2</sub> content is most likely related to inorganic minerals. This will be discussed in the following section.

**4.1.2. Effect of Mineral Composition on Residual CH<sub>4</sub> and CO<sub>2</sub>.** The mineral combinations in the oil shale samples are mainly quartz, clay, and carbonate minerals. The quartz content in the YJ oil shale is higher than in the FS oil shale, while the clay and carbonate mineral content is lower than in the FS oil shale. The relationships between the three minerals and the absolute volume of residual CH<sub>4</sub> and CO<sub>2</sub> are analyzed. The residual CH<sub>4</sub> and CO<sub>2</sub> are discussed separately.

Similar to the correlation between TOC and residual CH<sub>4</sub> content in FS oil shales, the impact of each mineral on residual CH<sub>4</sub> can be almost negligible due to the minimal volume of CH<sub>4</sub> (0.0001–0.0008 mL/g) (Figure 9). On the contrary, a positive correlation is presented between the residual CH<sub>4</sub> content and quartz in YJ oil shales (Figure 9a). Meanwhile, the quartz and TOC contents in YJ oil shales show a synergistic change (Figure 10a). Based on these consistent correlations, it is suggested that the influence mechanism of quartz on residual CH<sub>4</sub> in the YJ oil shale may be analogous to organic matter, where the intergranular pores of quartz particles are filled by asphaltenes, and residual CH<sub>4</sub> dissolved in them. However, the residual CH<sub>4</sub> content negatively correlates with clay and carbonate minerals (Figure 9b, c). This situation suggests that clay and carbonate minerals in YJ oil shales are unfavorable for preserving residual CH<sub>4</sub>. In addition, the correlation between TOC content and clay is not apparent (Figure 10b), while mutual inhibition with carbonate minerals is observed (Figure 10c), which implies that the increase of carbonate minerals will reduce the abundance of organic matter, thereby reducing the generation of CH<sub>4</sub>. The hydrophilicity of clay minerals needs to be considered, which will reduce gas adsorption capacity.<sup>47</sup> In the experimental samples with moisture equilibrated, moisture may occupy the adsorption sites, resulting in the microporous adsorption sites not being adsorbed by CH<sub>4</sub>.

The absolute volume of residual CO<sub>2</sub> released from FS oil shales only increases with carbonate (Figure 11c) but shows a negative correlation and irrelevance with quartz and clay minerals (Figure 11a, b), respectively. Combined with the previous conclusion that TOC is not a dominant controlling factor of residual CO<sub>2</sub> content in the FS oil shale, it suggests that the residual CO<sub>2</sub> is probably of inorganic origin related to carbonate minerals. The higher the content of carbonate minerals, the more the residual CO<sub>2</sub> is released after crushing. However, the carbon isotope test has not been carried out. Evidence of CO<sub>2</sub> genesis will be provided in future research.

However, the correlation between residual CO<sub>2</sub> released from YJ oil shales and mineral components is opposite to that of FS oil shales but similar to the change of residual CH<sub>4</sub> in YJ oil shales. Both are positively correlated with quartz and negatively correlated with carbonate and clay minerals (Figure 11). Therefore, the preservation mechanism of residual CO<sub>2</sub> in

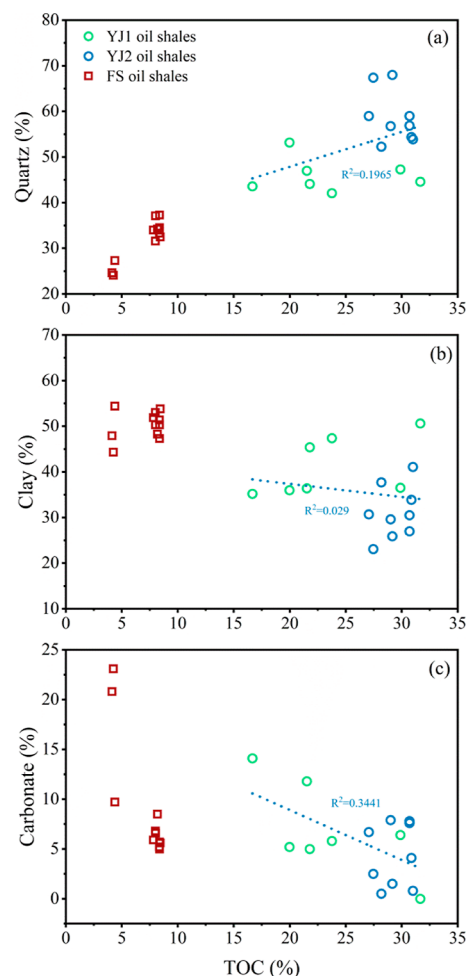


**Figure 10.** Relationships between TOC contents and (a) quartz, (b) clay, and (c) carbonate minerals of oil shale samples.

the YJ oil shale is identical to that of CH<sub>4</sub>. CO<sub>2</sub> would also dissolve in the asphaltenes filled with the intergranular pores of quartz particles. Although clays have excellent surface areas and can adsorb methane to their internal structure,<sup>56</sup> there is a negative correlation between residual CO<sub>2</sub> and clays in this study, similar to CH<sub>4</sub>. Therefore, in the moisture-equilibrated oil shale samples, the adsorption of CH<sub>4</sub> and CO<sub>2</sub> on clay minerals is not essential. These further illustrate that the residual CH<sub>4</sub> and CO<sub>2</sub> in the YJ oil shale are held in matrix bituminite as solutes, and their yield is mainly controlled by the organic matter content. Additionally, based on the negative correlation that the clay and carbonate minerals showed with TOC content in Figure 10b,c, it is considered that the increase of clay and carbonate minerals will dilute the TOC content in YJ oil shales, consequently reducing the generation and release of residual CH<sub>4</sub> and CO<sub>2</sub>. It is an adverse factor in natural gas production. Nevertheless, it will reduce the GHG emissions during the oil shale crushing process from the perspective of GHG emission reduction.

**4.2. Effect of the Pore Structure on the Release of Residual CH<sub>4</sub> and CO<sub>2</sub>.** The research on the pore structure of shale after releasing the residual gas revealed that the residual gas was chiefly released from the mesopores and macropores.<sup>28</sup> It declared that the storage and release of residual gas are closely related to the pore structure. The pores of oil shale are related to organic matter and porous minerals. It has been

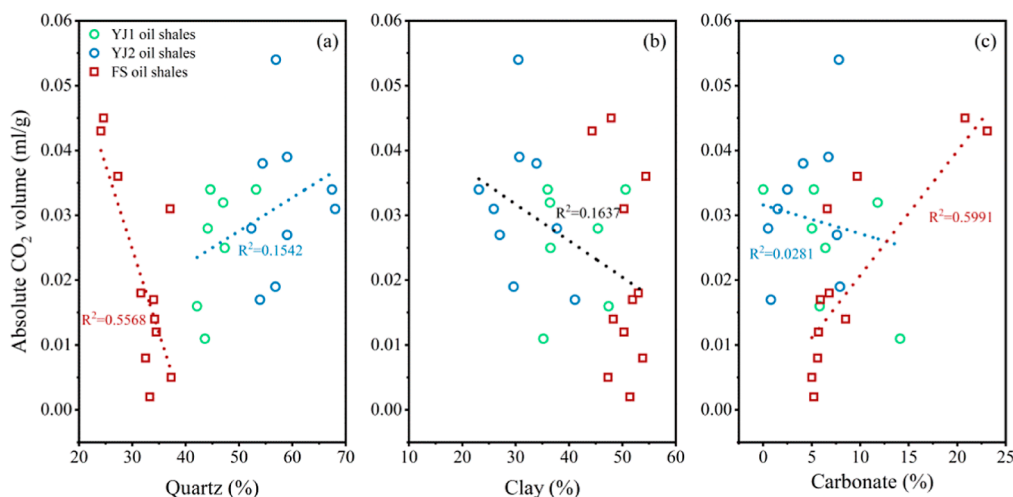


**Figure 11.** Relationships between the absolute CO<sub>2</sub> volume in residual gas and (a) quartz, (b) clay, and (c) carbonate content of oil shale samples.

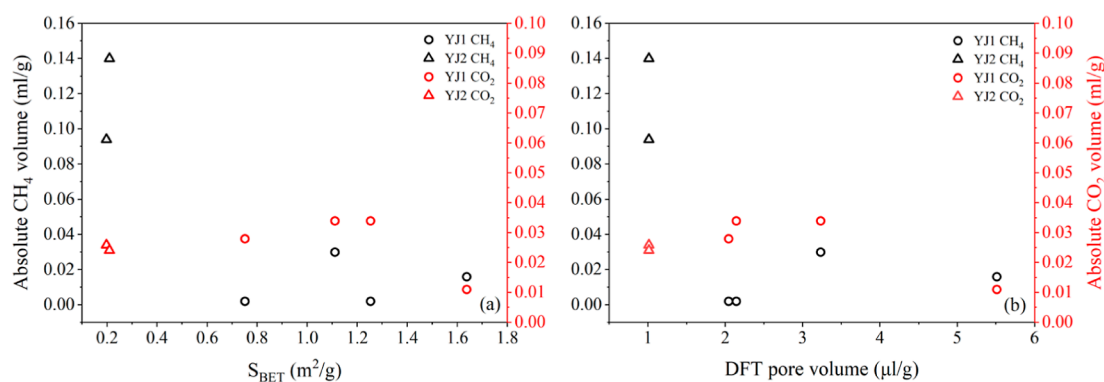


**Figure 12.** Relationships between the absolute volume of residual CH<sub>4</sub> and CO<sub>2</sub> and the pore structure in YJ oil shales: (a) BET specific surface area; (b) DFT pore volume.

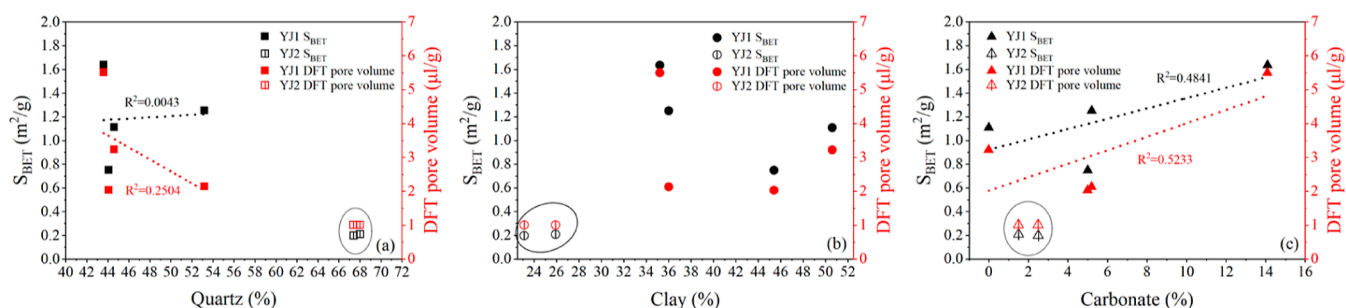


**Figure 13.** Relationships between main minerals and the pore structure in YJ oil shales: (a) quartz, (b) clay, and (c) carbonate.

confirmed that the organic pores are not developed in YJ and FS oil shale samples, so the effect of organic pores on the release of residual CH<sub>4</sub> and CO<sub>2</sub> is not discussed here.

Figure 12 displays the relationship between the absolute volumes of residual CH<sub>4</sub> and CO<sub>2</sub> and the pore structure in the YJ oil shales. Negative trends are observed between the amount of residual CH<sub>4</sub> and CO<sub>2</sub> released and the surface area and total pore volume, which further suggests that the residual CH<sub>4</sub> and CO<sub>2</sub> released from the YJ oil shale are dissolved in the asphaltene filling the pore space, resulting in a negative correlation between the amount of CH<sub>4</sub> and CO<sub>2</sub> released and the pore structure (both micropore and total pore space).

The correlation analysis between the minerals and pore structure in the YJ oil shale in Figure 13 shows that the

carbonates in the YJ1 oil shale also contribute to the development of total pores; while quartz is unfavorable for the development of pores, the correlation between clays and pores is not apparent. Based on the relationship between residual gas and mineral components, the residual CH<sub>4</sub> and CO<sub>2</sub> only positively correlate with quartz, which indicates that quartz can initially provide pore space. However, due to the occupation of the skeleton space by asphaltene, the contribution of quartz to pores is masked. Although carbonate minerals contribute to pores, they are not the primary storage space of residual CH<sub>4</sub> and CO<sub>2</sub> in the YJ oil shale. In addition, the organic matter content and thermal maturity of the YJ2 oil shale are higher than those of the YJ1 oil shale (Table 2), thus more asphaltenes were produced and filled in the micropores

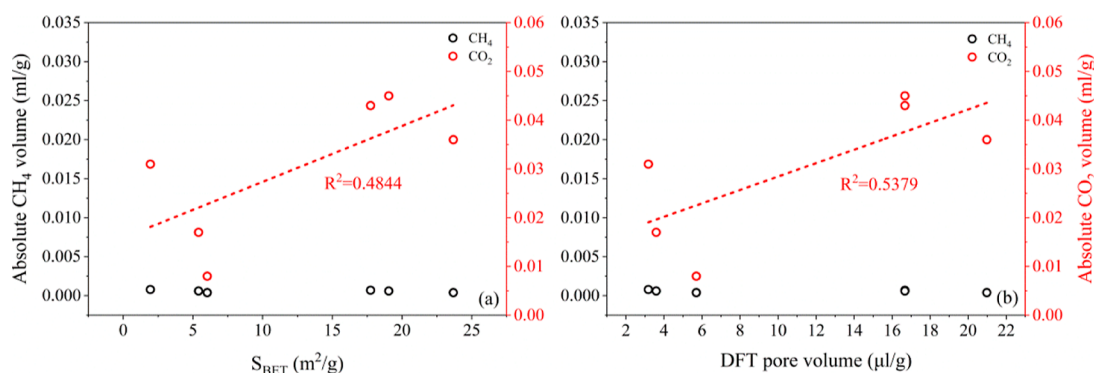


**Figure 14.** Relationships between the absolute volume of residual  $\text{CH}_4$  and  $\text{CO}_2$  and the pore structure in FS oil shales: (a) BET specific surface area; (b) DFT pore volume.

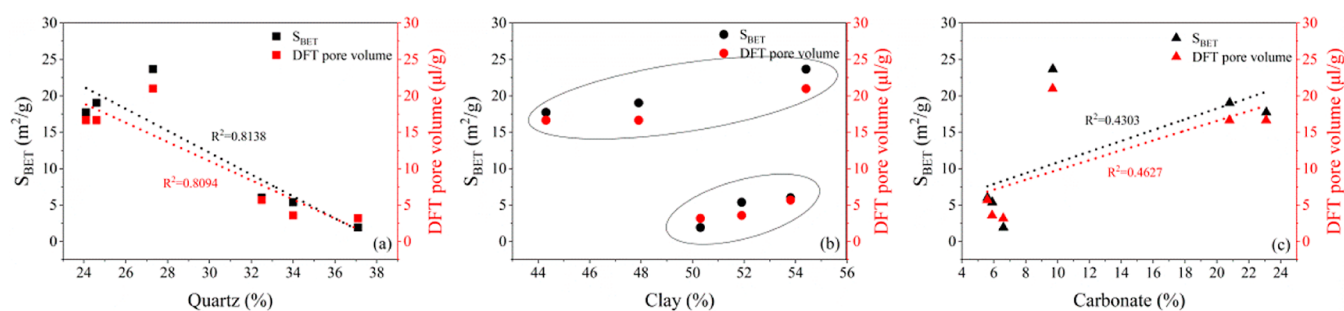


**Figure 15.** Relationships between main minerals and the pore structure in FS oil shales: (a) quartz, (b) clay, and (c) carbonate.

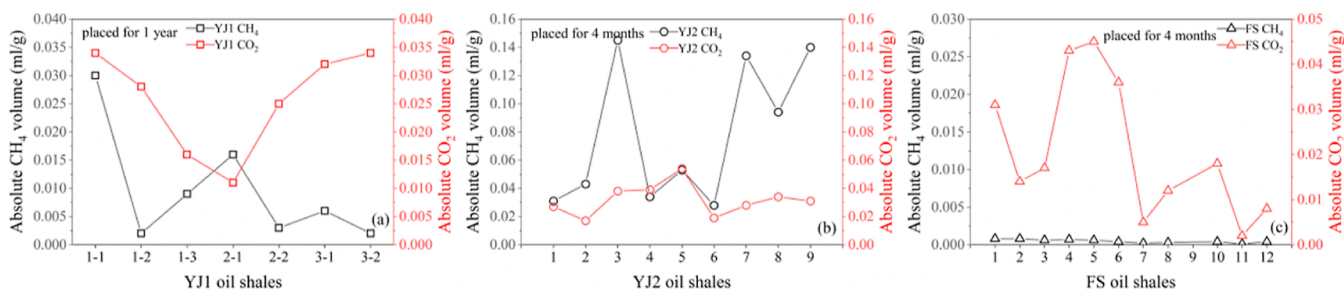


**Figure 16.** Variation characteristics of the absolute release of residual  $\text{CH}_4$  and  $\text{CO}_2$  from oil shale with storage time and particle size. (a) YJ1 oil shales. Samples YJ1-1-1, YJ1-1-2, and YJ1-1-3: >65 mm; samples YJ1-2-1 and YJ1-2-2: 8–65 mm; samples YJ1-3-1 and YJ1-3-2: <8 mm; (b) YJ2 oil shales. Samples YJ2-1 to YJ2-9: >65 mm; and (c) FS oil shales. FS-1 to FS-12: >65 mm.

of the YJ2 oil shale, resulting in minimal surface area and pore volume. Consequently, the filling of pores by asphaltenes leads to the cover-up of the impact of pore structure on residual  $\text{CH}_4$  and  $\text{CO}_2$  content.

Unlike YJ oil shales, the residual  $\text{CH}_4$  volume in FS oil shales does not correlate with the pore structure because the  $\text{CH}_4$  volume is too small. In contrast, there is a strong positive linear correlation between the residual  $\text{CO}_2$  volume and the surface area and pore volume (Figure 14). According to the PSD characteristics of the FS oil shale (Figure 4c), the residual  $\text{CO}_2$  released from the FS oil shale is strongly linked to micropores and mesopores. Furthermore, the previous section concluded that residual  $\text{CO}_2$  in the FS oil shale increases with the carbonate minerals. Then, if carbonates can contribute micropores and mesopores, it can be proven that the residual  $\text{CO}_2$  released from the FS oil shale is stored in the intergranular or intercrystalline pores provided by carbonate minerals.

Figure 15 shows an apparent positive linear correlation between carbonate minerals and surface area and DFT pore

volume in the FS oil shale and a slight upward trend between clays and them as a whole, but there are two regions with evident high and low values. It means that the carbonates can provide micropores and mesopores, while the contribution of clays to pores is uncertain. Therefore, it can be determined that the residual  $\text{CO}_2$  released from the FS oil shale is mainly stored in the intergranular or intragranular pores of carbonate minerals. Previous research has also reported the same storage mode of residual  $\text{CH}_4$  in the Wufeng-Longmaxi Formation shale.<sup>26</sup> However, a strong negative correlation between quartz and surface area and DFT pore volume is presented, indicating that quartz is unfavorable for developing nanopores in FS oil shales. This is consistent with the relationship between the quartz and pore structure in the shale of the Qingshankou Formation in the Songliao Basin.<sup>50</sup>

**4.3. Effects of Storage Time and Particle Sizes on the Release of Residual  $\text{CH}_4$  and  $\text{CO}_2$  from Oil Shale.** The particle size information on oil shale samples is shown in Table 1. As shown in Figure 16a, the residual  $\text{CH}_4$  contents are almost lower than the amount of  $\text{CO}_2$  released from seven YJ1

oil shale samples placed for one year with different grain sizes, while the grain size has little influence on the release of CH<sub>4</sub> and CO<sub>2</sub>. In contrast, the residual CH<sub>4</sub> contents are generally higher than CO<sub>2</sub> (Figure 16b) released from YJ2 oil shale samples placed for four months and are also higher than the residual CH<sub>4</sub> released from the YJ1 oil shale. According to the results, it can be concluded that the residual CH<sub>4</sub> in oil shale is easier to escape than CO<sub>2</sub> with the extension of the storage time. It further illustrates the conclusion in 4.1.1 that CO<sub>2</sub> has a more substantial adsorption capacity than CH<sub>4</sub> in matrix bituminite. Furthermore, since the organic matter content and thermal maturity of the YJ2 oil shale are higher than those of the YJ1 oil shale, more CH<sub>4</sub> can be generated during geological evolution and retained in the oil shale layers.

For the FS oil shales that have been stored for four months, however, the residual CH<sub>4</sub> content released after crushing is greatly low, while the residual CO<sub>2</sub> content is comparable to that of YJ oil shales (Figure 16c). This is because the organic matter in the FS oil shale is immature and the content is relatively low; additionally, the type of organic matter is more inclined to generate oil, so it is not sufficient to produce CH<sub>4</sub> in large quantities. However, the residual CO<sub>2</sub> is less affected by organic matter since it is probably inorganic genesis related to carbonate minerals.

In summary, we believe that for organic-rich and mature oil shale, the residual CH<sub>4</sub> and CO<sub>2</sub> are continuously emitted during the mining and crushing process before retorting and that residual CH<sub>4</sub> is emitted at a faster rate than CO<sub>2</sub>. However, oil shales with relatively low organic matter content and immature evolution emit less residual CH<sub>4</sub> but still retain significant amounts of CO<sub>2</sub> that can be released to the atmosphere during crushing. Therefore, it is recommended that oil shale be processed and utilized as soon as possible to avoid more GHG emissions into the atmosphere.

**4.4. Estimation of GHG Emissions during Oil Shale Crushing in the Study Area.** According to the simulation experiment results for quantitative calculation of GHG emissions from the oil shale crushing process, the average CH<sub>4</sub> emission during the YJ oil shale crushing was 0.048 m<sup>3</sup>/t, and the average CO<sub>2</sub> emission was 0.029 m<sup>3</sup>/t. Using the CH<sub>4</sub> and CO<sub>2</sub> density values of 0.68 kg/m<sup>3</sup> and 1.86 kg/m<sup>3</sup> at a standard atmospheric pressure of 15 °C, the volume is converted to mass as CH<sub>4</sub> emissions of 0.033 kg/t<sub>oil shale</sub> and CO<sub>2</sub> emissions of 0.054 kg/t<sub>oil shale</sub>, respectively. The YJ oil shale plant extracts (crushes) approximately 1 million tons/year of oil shale annually, so the annual CH<sub>4</sub> and CO<sub>2</sub> emissions from crushing are 33 and 54 t/y, respectively.

The average CH<sub>4</sub> and CO<sub>2</sub> emissions during the crushing process of the FS oil shale are 0.0005 m<sup>3</sup>/t and 0.021 m<sup>3</sup>/t, respectively. Converted to mass, the CH<sub>4</sub> emission is 0.00034 kg/t<sub>oil shale</sub> and the CO<sub>2</sub> emission is 0.039 kg/t<sub>oil shale</sub>, respectively. The FS Shale Refinery extracts (crushes) approximately 14 million tons/y of oil shale annually, so the annual CH<sub>4</sub> and CO<sub>2</sub> emissions from crushing are 4.76 and 546 t/y, respectively.

In order to reduce GHG emissions during the oil shale mining process, two aspects can be considered: first, the construction of closed crushing systems and gas extraction facilities in the mining area to realize zero emission of GHGs and dust; second, the YJ mining area can be considered for the adoption of advanced underground in situ conversion process (ICP) technology,<sup>57,58</sup> which can effectively reduce the GHG emissions in the process of oil shale mining and utilization.

## 5. CONCLUSIONS

The quantitative calculation of GHG release after oil shale crushing and the analysis of its main controlling factors were carried out in a set of oil shale samples with different organic matter contents and maturity. The obtained results show that the TOC content and maturity are the primary controlling factors of residual CH<sub>4</sub> release. Among the studied samples, the YJ oil shale that was organic-rich (type II<sub>2</sub> organic matter) and entered the oil window had the highest residual CH<sub>4</sub> release, ranging from 0.002 to 0.145 mL/g, while the relatively poor organic matter (type II<sub>1</sub> organic matter) and immature FS oil shale had the lowest residual CH<sub>4</sub> release, ranging from 0.0001 to 0.0008 mL/g. The amount of residual CO<sub>2</sub> released from YJ and FS oil shales was comparable, which is 0.011–0.054 and 0.002–0.045 mL/g, respectively. However, the controlling factors in different oil shales were various. The former was positively correlated with TOC, but the latter was positively correlated with carbonate minerals and the pores they provide. It indicates that the residual CO<sub>2</sub> released from the FS oil shale was stored in the intergranular or intercrystalline pores of carbonate minerals and was likely to be of inorganic origin.

Due to the blockage of organic and inorganic pores in the YJ oil shale, the correlations between the residual CH<sub>4</sub> and CO<sub>2</sub> volume and pore structure differed from the traditional understanding. It is a vital gas preservation mechanism for the YJ oil shale in which residual CH<sub>4</sub> and CO<sub>2</sub> dissolve in matrix asphaltenes as solutes. Moreover, the absorption capacity of CO<sub>2</sub> was more significant than that of CH<sub>4</sub>, which is one of the reasons the release of residual CO<sub>2</sub> was lower than that of CH<sub>4</sub> during the same crushing time. The increase in clay and carbonate minerals in YJ oil shales will dilute the TOC content, thereby reducing the generation and release of CH<sub>4</sub> and CO<sub>2</sub>.

As the storage time increases, the residual CH<sub>4</sub> preferentially escapes into the atmosphere from organic-rich and mature oil shale. However, whether mature or immature, a large amount of CO<sub>2</sub> remains in the oil shale, which can be released into the atmosphere during crushing. The particle size of oil shale had little influence on the release of residual CH<sub>4</sub> and CO<sub>2</sub>.

## ■ ASSOCIATED CONTENT

### Data Availability Statement

The data used to support the findings of this study are included within the article and available from the corresponding author upon request.

## ■ AUTHOR INFORMATION

### Corresponding Author

Lijuan Wang – Northwest Institute of Eco-Environment and Resources, Chinese Academy of Sciences, Lanzhou 730000, China; Key Laboratory of Petroleum Resources, Gansu Province, Lanzhou 730000, China; University of Chinese Academy of Sciences, Beijing 100049, China; [orcid.org/0009-0007-6815-4590](https://orcid.org/0009-0007-6815-4590); Email: [Wangljy@163.com](mailto:Wangljy@163.com)

### Authors

Yingxin Lu – Northwest Institute of Eco-Environment and Resources, Chinese Academy of Sciences, Lanzhou 730000, China; Key Laboratory of Petroleum Resources, Gansu Province, Lanzhou 730000, China; University of Chinese Academy of Sciences, Beijing 100049, China

**Guojun Chen** – Northwest Institute of Eco-Environment and Resources, Chinese Academy of Sciences, Lanzhou 730000, China; Key Laboratory of Petroleum Resources, Gansu Province, Lanzhou 730000, China; University of Chinese Academy of Sciences, Beijing 100049, China

**Lianhua Xue** – Northwest Institute of Eco-Environment and Resources, Chinese Academy of Sciences, Lanzhou 730000, China; Key Laboratory of Petroleum Resources, Gansu Province, Lanzhou 730000, China

**Zhongning Zhang** – Northwest Institute of Eco-Environment and Resources, Chinese Academy of Sciences, Lanzhou 730000, China; Key Laboratory of Petroleum Resources, Gansu Province, Lanzhou 730000, China

**Shuan Wang** – Gansu Yaojie Oil Shale Comprehensive Utilization Co., Ltd., Lanzhou 730080, China

**Jian Gao** – Shale Oil Plant of Fushun Mining Group Co., Ltd., Fushun 113000, China

Complete contact information is available at:

<https://pubs.acs.org/10.1021/acsomega.4c00435>

## Notes

The authors declare no competing financial interest.

## ACKNOWLEDGMENTS

This research was supported by the National Nature Science Foundation of China (grant no. 41975117).

## REFERENCES

- (1) Malhotra, R. In *Fossil Energy. In Oil Shale Processing, Chemistry and Technology*; Oja, V., Suuberg, E. M., Eds.; Springer, 2013; pp 99–148.
- (2) Zou, C. Unconventional Petroleum Geology In *Oil Shale*, 2nd ed.; Zou, C., Ed.; Elsevier Inc, 2017; pp 371–389.
- (3) Dyni, J. R. Geology and resources of some world oil-shale deposits. *Oil Shale* **2003**, *20* (3), 193–252.
- (4) Yu, F.; Sun, P.; Zhao, K. a.; Ma, L.; Tian, X. Experimental constraints on the evolution of organic matter in oil shales during heating: Implications for enhanced in situ oil recovery from oil shales. *Fuel* **2020**, *261*, 116412.
- (5) Xu, S.; Sun, Y.; Lü, X.; Yang, Q.; Li, Q.; Wang, Z.; Guo, M. Effects of composition and pore evolution on thermophysical properties of Huadian oil shale in retorting and oxidizing pyrolysis. *Fuel* **2021**, *305* (3), 121565.
- (6) Jiang, X.; Han, X.; Cui, Z. New technology for the comprehensive utilization of Chinese oil shale resources. *Energy* **2007**, *32* (5), 772–777.
- (7) Külaots, I.; Goldfarb, J. L.; Suuberg, E. M. Characterization of Chinese, American and Estonian oil shale semicokes and their sorptive potential. *Fuel* **2010**, *89* (11), 3300–3306.
- (8) Yang, Q.; Li, X.; Qian, Y.; Zhang, D. Technical and economic analysis of an oil shale comprehensive utilization process with solid heat carrier technology. *Carbon Resour. Convers.* **2018**, *1* (3), 266–272.
- (9) Zhao, J.; Wang, L.; Yang, D.; Kang, Z. Characteristics of oil and gas production of oil shale pyrolysis by water vapor injection. *Oil Shale* **2022**, *39* (3), 153–168.
- (10) Zhang, H.; Wei, P.; Wang, T.; Lin, W.; Zhang, J. Geochemistry characteristics of Natural gas in Minhe Basin (In Chinese). *Gas Ind.* **2005**, *25* (11), 10–13.
- (11) Zhang, C.; Xu, X.; Ma, D. Yaojie Formation Shale Reservoir Gas-bearing and Geochemical Characteristics in Yaojie Mine Area, Minhe Basin (In Chinese). *Coal Geology of China* **2015**, *27* (12), 29–32.
- (12) Ma, Y.; Zhang, Y.; Wang, Q.; Chen, C.; Zhong, N.; Han, H. The gas potential of Jurassic continental shale in the middle-small basins, Northwest China. *Chin. Sci. Bull.* **2014**, *59* (9), 809–815.
- (13) IPCC. *Climate Change 2022: Mitigation of Climate Change. Contribution of Working Group III to the Sixth Assessment Report of the Intergovernmental Panel on Climate Change, In 2022: Energy Systems*; Clarke, L., Wei, Y.-M., Navarro, A. D. L. V., Garg, A., Hahmann, A. N., Khennas, S., Azevedo, I. M. L., Löschel, A., Singh, A. K.; Steg, L., Eds.; Cambridge University Press, 2022.
- (14) Nduagu, E. L.; Gates, I. D. Unconventional Heavy Oil Growth and Global Greenhouse Gas Emissions. *Environ. Sci. Technol.* **2015**, *49* (14), 8824–8832.
- (15) Gavrilova, O.; Vilu, R.; Vallner, L. A life cycle environmental impact assessment of oil shale produced and consumed in Estonia. *Resour., Conserv. Recycl.* **2010**, *55* (2), 232–245.
- (16) Zhou, H.; Qian, Y.; Kraslawski, A.; Yang, Q.; Yang, S. Life-cycle assessment of alternative liquid fuels production in China. *Energy* **2017**, *139*, 507–522.
- (17) Zhou, H.; Yang, Q.; Zhu, S.; Song, Y.; Zhang, D. Life cycle comparison of greenhouse gas emissions and water consumption for coal and oil shale to liquid fuels. *Resour., Conserv. Recycl.* **2019**, *144*, 74–81.
- (18) Ren, X. *Study on the movement and gas emission law of the compound roof of coal seam and oil shale (in Chinese)*; Application study, Xi'an University of Science and Technology: Xi'an, Shaanxi, 2020.
- (19) Xiao, C.; Fu, B.; Shui, H.; Guo, Z.; Zhu, J. Detecting the Sources of Methane Emission from Oil Shale Mining and Processing Using Airborne Hyperspectral Data. *Remote Sens.* **2020**, *12* (3), 537.
- (20) Schatzel, S. J.; Cooke, G. A. Organic and mineralogic factors influencing Green River oil shale methane emissions. *Fuel* **1994**, *73* (4), 573–578.
- (21) Wang, G.; Ren, T.; Zhang, L.; Shu, L. Undersorbable residual gas in coal seams and its influence on gas drainage. *Int. J. Min. Sci. Technol.* **2017**, *27* (5), 763–769.
- (22) Siirde, A.; Elderermann, M.; Rohumaa, P.; Guska, J. Analysis of Greenhouse Gas Emissions from Estonian Oil Shale Based Energy Production Processes. Life Cycle Energy Analysis Perspective. *Oil Shale* **2013**, *30* (2S), 268–282.
- (23) Sundquist, E. T.; Miller, G. A. Oil Shales and Carbon Dioxide. *Science* **1980**, *208* (4445), 740–741.
- (24) Siirde, A.; Roos, I.; Martins, A. Estimation of Carbon Emission Factors for the Estonian Shale Oil Industry. *Oil Shale* **2011**, *28* (1S), 127–139.
- (25) Zhang, T.; Yang, R.; Milliken, K. L.; Ruppel, S. C.; Pottorf, R. J.; Sun, X. Chemical and isotopic composition of gases released by crush methods from organic rich mudrocks. *Org. Geochem.* **2014**, *73*, 16–28.
- (26) Wang, Q.; Shen, C.; Chen, Q.; Zhang, L.; Lu, H. Pore Characteristics and Gas Released by Crush Methods of Wufeng-Longmaxi Shale in the Northwest of Hubei Province, China. *Acta Geol. Sin.* **2015**, *89*, 93–96.
- (27) Wu, C.; Tuo, J.; Zhang, M.; Sun, L.; Qian, Y.; Liu, Y. Sedimentary and residual gas geochemical characteristics of the Lower Cambrian organic-rich shales in Southeastern Chongqing, China. *Mar. Pet. Geol.* **2016**, *75*, 140–150.
- (28) Liang, M.; Wang, Z.; Zheng, G.; Christopher Greenwell, H.; Li, H.; Zhang, L.; Feng, X.; Zhang, K. Occurrence and influence of residual gas released by crush methods on pore structure in Longmaxi shale in Yangtze Plate, Southern China. *China Geol.* **2020**, *3* (4), 545–557.
- (29) Wang, T.; Wang, Q.; Liu, W.; Lu, H.; Liu, D. Quantitative Method of Crushed Gas in shale and Its Geological Significance (In Chinese). *J. Jilin Univ., Earth Sci. Ed.* **2018**, *48* (6), 1645–1653.
- (30) Abouna, S. Greenhouse gas emissions from shallow uncovered coal seams. *Int. J. Min. Sci. Technol.* **2014**, *24* (3), 341–344.
- (31) Yang, H.; Han, B.; Qian, Z. Determination principle of residual Gas and Analysis of influencing factors on the results of Laboratory Measurement. *IOP Conf. Ser.: Earth Environ. Sci.* **2020**, *526*, 012056.
- (32) Li, J.; Qin, R. The characteristics of oil shale and the controlling factors of metallogeny in the Yaojie oil shale ore-bearing area (In Chinese). *Coal Chem. Ind.* **2018**, *41* (4), 43–47.

- (33) Liu, Z.; Liu, R.; Sun, P.; Meng, Q.; Hu, F. Oil shale characteristics and distribution in typical basins of China (In Chinese). *J. Jilin Univ., Earth Sci. Ed.* **2020**, *50* (02), 313–325.
- (34) Han, H.; Pang, P.; Zhong, N.; Luo, Q.; Ma, Y.; Gao, Y. The pore characteristics and gas potential of the Jurassic continental shales in the middle-small basins, northwest China. *J. Pet. Sci. Eng.* **2020**, *188*, 106873.
- (35) Xu, S.; Liu, Z.; Dong, Q.; Liu, S.; Liu, R.; Meng, Q. Eocene sedimentary evolution and its control over coal & oil shale development in Fushun Coalfield (In Chinese). *J. China Univ. Pet., Ed. Nat. Sci.* **2012**, *36* (02), 45.
- (36) Li, J.; Zhou, S.; Li, Y.; Ma, Y.; Yang, Y.; Li, C. Effect of organic matter on pore structure of mature lacustrine organic-rich shale: A case study of the Triassic Yanchang shale, Ordos Basin, China. *Fuel* **2016**, *185*, 421–431.
- (37) Sing, K. S. W.; Everett, D. H.; Haul, R. A. W.; Mescou, L.; Pierotti, R. A.; Rouquerol, J.; Siemieniewska, T. Reporting physisorption data for gas/solid systems with special reference to the determination of surface area and porosity (Recommendations 1984). *Pure Appl. Chem.* **1985**, *57* (4), 603–619.
- (38) Pang, P.; Han, H.; Hu, L.; Guo, C.; Gao, Y.; Xie, Y. The calculations of pore structure parameters from gas adsorption experiments of shales: Which models are better? *J. Nat. Gas Sci. Eng.* **2021**, *94*, 104060.
- (39) Zhang, Z.; Yang, Z. Theoretical and practical discussion of measurement accuracy for physisorption with micro- and mesoporous materials. *Chin. J. Catal.* **2013**, *34* (10), 1797–1810.
- (40) Han, H.; Liu, P.; Ding, Z.; Shi, P.; Jia, J.; Zhang, W.; Liu, Y.; Chen, S.; Lu, J.; Chen, K.; et al. The Influence of Extractable Organic Matter on Pore Development in the Late Triassic Chang 7 Lacustrine Shales, Yanchang Formation, Ordos Basin, China. *Acta Geol. Sin.* **2018**, *92* (4), 1508–1522.
- (41) Li, L.; Liu, Y.; Wang, X.; Zhang, M.; Cao, C.; Xing, I. Development of a Combined Device with High Vacuum and Pulsed Discharge Gas Chromatography and Its Application in Chemical Analysis of Gases from Rock Samples (In Chinese). *Rock Miner. Anal.* **2017**, *36* (3), 222–230.
- (42) Tissot, B. P.; Welte, D. H. *Petroleum Formation and Occurrence*, 2nd ed.; Springer-Verlag, 1984.
- (43) Thommes, M.; Kaneko, K.; Neimark, A. V.; Olivier, J. P.; Rodriguez-Reinoso, F.; Rouquerol, J.; Sing, K. S. W. Physisorption of gases, with special reference to the evaluation of surface area and pore size distribution (IUPAC Technical Report). *Pure Appl. Chem.* **2015**, *87* (9–10), 1051–1069.
- (44) Schrodt, J.; Ocampo, A. Variations in the pore structure of oil shales during retorting and combustion. *Fuel* **1984**, *63* (11), 1523–1527.
- (45) Bai, F.; Sun, Y.; Liu, Y.; Guo, M. Evaluation of the porous structure of Huadian oil shale during pyrolysis using multiple approaches. *Fuel* **2017**, *187*, 1–8.
- (46) Chalmers, G. R. L.; Bustin, R. M. Lower Cretaceous gas shales in northeastern British Columbia, Part I geological controls on methane sorption capacity. *Bull. Can. Pet. Geol.* **2008**, *56* (1), 1–21.
- (47) Ross, D. J. K.; Bustin, R. M. Shale gas potential of the Lower Jurassic Gordondale Member, northeastern British Columbia, Canada. *Bull. Can. Pet. Geol.* **2007**, *55* (1), 51–75.
- (48) Zhang, T.; Ellis, G. S.; Ruppel, S. C.; Milliken, K.; Yang, R. Effect of organic-matter type and thermal maturity on methane adsorption in shale-gas systems. *Org. Geochem.* **2012**, *47* (6), 120–131.
- (49) Ross, D. J. K.; Marc Bustin, R. The importance of shale composition and pore structure upon gas storage potential of shale gas reservoirs. *Mar. Pet. Geol.* **2009**, *26* (6), 916–927.
- (50) Zeng, W.; Song, Z. Influences of Clay Mineral and Organic Matter on Nanoscale Pore Structures of the Cretaceous Lacustrine Shales in the Songliao Basin, Northeast China. *Energies* **2022**, *15* (19), 7075.
- (51) Cheng, A.-L.; Huang, W.-L. Selective adsorption of hydrocarbon gases on clays and organic matter. *Org. Geochem.* **2004**, *35* (4), 413–423.
- (52) Svrcek, W. Y.; Mehrotra, A. K. Gas solubility, viscosity and density measurements for Athabasca bitumen. *J. Can. Pet. Technol.* **1982**, *21* (04), 31–38.
- (53) Robert, P. Classification of organic matter by means of fluorescence; Application to hydrocarbon source rocks. *Int. J. Coal Geol.* **1981**, *1* (2), 101–137.
- (54) Gensterblum, Y.; Busch, A.; Krooss, B. M. Molecular concept and experimental evidence of competitive adsorption of H<sub>2</sub>O, CO<sub>2</sub> and CH<sub>4</sub> on organic material. *Fuel* **2014**, *115*, 581–588.
- (55) Cheng, Y.; Lin, S.; Ma, Y. Pore Structure of Oil Shale Heated by Using Conduction and Microwave Radiation: A Case Study of Oil Shale from the Fushun in China. *Geofluids* **2022**, *2022*, 1–14.
- (56) Venaruzzo, J. L.; Volzone, C.; Rueda, M. L.; Ortega, J. Modified bentonitic clay minerals as adsorbents of CO, CO<sub>2</sub> and SO<sub>2</sub> gases. *Microporous Mesoporous Mater.* **2002**, *56* (1), 73–80.
- (57) Crawford, P. M.; Killen, J. C. New challenges and directions in oil shale development technologies. *ACS Symp. Ser.* **2010**, *1032*, 21–60.
- (58) Kang, Z.; Zhao, Y.; Yang, D.; Tian, L.; Li, X. A pilot investigation of pyrolysis from oil and gas extraction from oil shale by in-situ superheated steam injection. *J. Pet. Sci. Eng.* **2020**, *186*, 106785.